ACS NANO

www.acsnano.org

ARTICLE

Easy and Versatile Synthesis of Bulk Quantities of Highly Enriched ^{13}C-Graphene Materials for Biological and Safety Applications

Viviana González, Javier Frontiñan-Rubio, M. Victoria Gomez, Tiziano Montini, Mario Durán-Prado, Paolo Fornasiero, Maurizio Prato,* and Ester Vázquez*

Cite This: *ACS Nano* 2023, 17, 606–620

Read Online

ACCESS | Metrics & More | Article Recommendations | Supporting Information

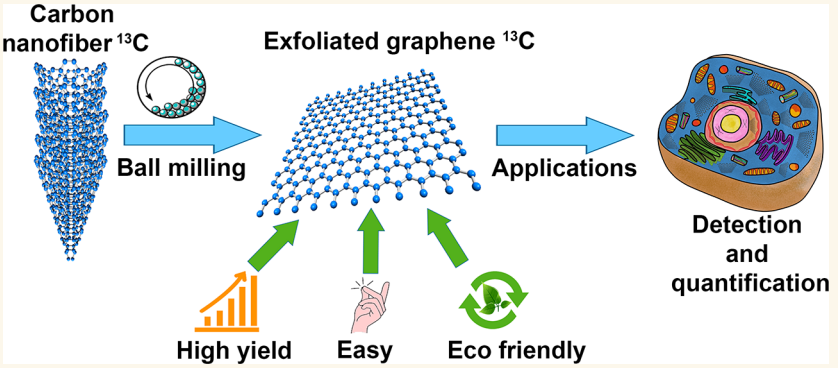

ABSTRACT: The preparation of bulk quantities of ^{13}C-labeled graphene materials is relevant for basic investigations and for practical applications. In addition, ^{13}C-labeled graphene materials can be very useful in biological and environmental studies, as they may allow the detection of graphene or its derivatives in cells or organs. In this paper, we describe the synthesis of ^{13}C-labeled graphene materials (few-layer graphene, FLG, and graphene oxide, GO) on a tens of mg scale, starting from ^{13}C-labeled methane to afford carbon fibers, followed by liquid-phase exfoliation (FLG) or oxidation (GO). The materials have been characterized by several analytical and microscopic techniques, including Raman and nuclear magnetic resonance spectroscopies, thermogravimetric analysis, X-ray photoelectron spectroscopy, and X-ray powder diffraction. As a proof of concept, the distribution of the title compounds in cells has been investigated. In fact, the analysis of the ^{13}C/^{12}C ratio with isotope ratio mass spectrometry (IRMS) allows the detection and quantification of very small amounts of material in cells or biological compartments with high selectivity, even when the material has been degraded. During the treatment of ^{13}C-labeled FLG with HepG2 cells, 4.1% of the applied dose was found in the mitochondrial fraction, while 4.9% ended up in the nuclear fraction. The rest of the dose did not enter into the cell and remained in the plasma membrane or in the culture media.

KEYWORDS: *^{13}C-graphene material, bulk quantities, detection, quantification, safety applications*

2D nanomaterials are under intense investigation for applications in many fields of development.[1] In biological applications, the possibility of these materials to interact, at the nanoscale level, with biological entities gives rise to innovative approaches such as the creation of innovative therapeutic agents or the development of alternative theranostic approaches.[2] Nevertheless, real-life advances in this area rely on the investigations of the mechanisms with which these materials interact with cells, organs, or other

Received: October 2, 2022
Accepted: December 12, 2022
Published: December 20, 2022

Downloaded via 151.36.75.176 on August 31, 2023 at 06:10:17 (UTC).
See https://pubs.acs.org/sharingguidelines for options on how to legitimately share published articles.

© 2022 The Authors. Published by American Chemical Society

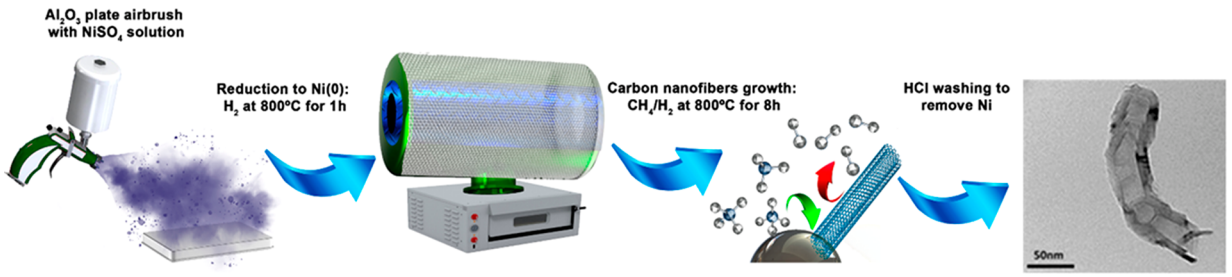

Figure 1. Schematic representation of the synthesis of carbon nanofibers. On the right: typical TEM image of the produced fibers.

biological compartments and their environment.[3] Another important issue is that state-of-the-art nanomaterials still generate toxicological concerns:[4] their end-use and the commercialization of final devices for any particular purpose depend on safety assessments to exclude possible hazards and risks for human health or for the environment, including the determination of exposure limits.[5] A particular challenge for nanosafety studies is to detect minimal amounts of 2D nanomaterials in complex biological and environmental contexts.[6,7] For metal-containing materials, the quantification can be achieved relatively easily by standard analytical techniques, such as inductively coupled plasma mass spectrometry (ICP-MS).[8] However, the quantitative determination of graphene materials is much more difficult, as these materials are mostly composed of carbon atoms and, in lesser amounts, of oxygen and hydrogen atoms, which are the same elements found in the environment or in living systems.[9]

Graphene materials are usually detected by microscopy techniques and Raman spectroscopy. Black, semi-transparent shapes in the transmission electron microscopy (TEM) or confocal microscopy images of biological cross sections are associated with graphene flakes,[10] while the detection of D- and G-bands in Raman spectra of natural samples is correlated to the presence of the 2D material.[11] However, even considering only detection without quantification, these techniques are insufficient, mainly because (i) once inside the biological tissues or the natural backgrounds, graphene materials can be degraded[12] and transformed to structurally and/or chemically different amorphous species which further complicate the recognition, and (ii) using these techniques, it is very difficult to locate the real position of the material within the different biological compartments. For these reasons, some authors have tried to label graphene materials with fluorescent organic labels or radioactive atoms,[4] but this modification changes the nature/surface of the nanomaterials and can affect their properties and their behavior. Moreover, quenching phenomena and/or detachment of these added moieties from the surface of the 2D nanomaterial can occur, thus making biological and environmental tracing unreliable.[13]

A different approach, very robust and reliable for nanosafety studies and for environmental tracing, is the use of isotope labeling of the graphene material itself.[14] Some studies have already reported the use of ^{14}C radioisotopes to describe the bioaccumulation and biotransformation of graphene in complex biological matrices.[15,16] However, a simpler concept is the employment of stable isotopes such as ^{13}C. ^{13}C- and ^{12}C-graphene materials synthesized by the same protocol have the same physicochemical properties and intrinsic behavior.[17] The analysis of the $^{13}C/^{12}C$ ratio with isotope ratio mass spectrometry (IRMS) allows the detection and quantification of very small amounts of material in a biological system or compartment, with high selectivity, even when this material has been degraded.[18] Moreover, although one of the main advantages of the use of radioactive isotopes such as ^{14}C is its quantification through imaging techniques, the use of ^{13}C magnetic resonance spectroscopic imaging (MRSI) is becoming progressively established.[19−21] Finally, stable isotope labeling avoids issues associated with the production of radioactive waste and approval of special experimental conditions when using radioactive materials for tracing.[22]

Some authors have already reported the preparation of ^{13}C-graphene materials,[23−25] mostly describing the physicochemical characteristics of graphene prepared by a chemical vapor deposition (CVD) process.[26−34] The cost of the ^{13}C starting materials and the low yield of the synthetic approaches usually prevent the preparation of bulk quantities of ^{13}C-graphene materials. However, the enrichment of bulk quantities of GO has also been described with around 7.1 atom% of ^{13}C atoms in the final GO, which has made it possible to investigate the bioaccumulation and toxicity of this 2D material in wheat.[35]

In this work, we detail an alternative approach for the production of readily available bulk quantities of ^{13}C-graphene materials, both graphene and GO, with different C/O ratios and lateral sizes, suitable for biological studies. The high ^{13}C% in the graphene materials (from 95 to 65%) has made it possible to trace graphene materials in individual cell compartments, such as the nucleus and the mitochondria. The protocol described herein will stimulate further investigations to quantify the biodistribution of graphene in different organisms and ecosystems and will permit studies of their biological degradation.

RESULTS AND DISCUSSION

The process leading to ^{13}C-graphene starts with the preparation of ^{13}C carbon fibers via a CVD process, which are then exfoliated by a standardized ball milling procedure.[36,37] Ball milling treatments show significantly lower environmental impact for the production of graphene[38] and can be easily scaled up in order to produce various graphene-related materials.[36,37,39,40] Our group has previously described that, following these treatments, the preparation of graphene can be achieved by exfoliation of graphite or carbon fibers.[41] In the present work, ^{12}C and ^{13}C nanomaterials have been prepared using carbon nanofibers obtained by a CVD process (see Methods). ^{12}C nanomaterials have been prepared as controls, and their physicochemical characterization has served to prove that ^{13}C labeling does not change the intrinsic structure nor the properties of the materials.

Synthesis of Carbon Nanofibers. Carbon nanofibers were grown by methane decomposition over Ni nanoparticles in a tubular furnace. Figure 1 presents, in a schematic way, the principal steps of the procedure: parameters such as amount of

https://doi.org/10.1021/acsnano.2c09799
ACS Nano 2023, 17, 606−620

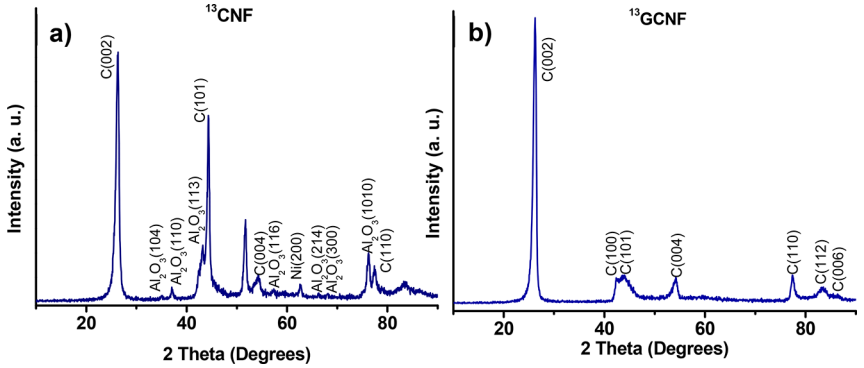

Figure 2. XRD spectra of (a) ^{13}C-CNF and (b) ^{13}C-GCNF.

Ni catalyst, concentration of CH_4 in the reaction mixture, gas flow, and reaction time for nanofiber growth were optimized to maximize the amount of carbon nanofibers obtained from each preparation. In a typical experiment,[42,43] carbon nanofibers were grown from a H_2/CH_4, 30/70 mixture (200 mL min^{-1}) over a Ni catalyst (obtained by reduction of $NiSO_4$ sprayed over Al_2O_3 plates) at 800 °C for 8 h. After cooling under Ar flow, the carbon nanofibers were washed in diluted HCl (to remove accessible Ni), water, and ethanol, finally yielding ^{12}C-CNF nanofibers. ^{13}C-CNF nanofibers were prepared following the same protocol but replacing CH_4 with $^{13}CH_4$. Fibers prepared in this way showed high quality by TEM. However, to eliminate any trace of nickel metal, the nanofibers were further graphitized at 2700 °C under helium atmosphere for 2 h with 0.5 bar overpressure.[41] The ^{12}C and ^{13}C graphitized carbon nanofibers were named as ^{12}C-GCNF and ^{13}C-GCNF, respectively. All samples were characterized using Raman spectroscopy, thermogravimetric analysis (TGA), elemental analysis, transmission electron microscopy (TEM), and X-ray powder diffraction (XRD).

Figure 2 shows the XRD spectra for ^{13}C-CNF and ^{13}C-GCNF in which the two peaks, at $2\theta = 26.39°$ and 42.44°, can be assigned as typical graphitic 002 and 101 planes, respectively. Through the 002 peak intensity plane, it is possible to determine the degree of crystallinity in carbon samples, using eq 1:[44]

$$G = \frac{3.461 - d_{002}}{3.461 - 3.352} \quad (1)$$

where 3.461 Å and 3.352 Å correspond to the d spacing for a fully turbostatic disordered and highly oriented pyrolytic graphite, respectively.

In general, graphitized nanofibers show a higher degree of crystallinity, determined by the d_{002} spacing peak (Table 1). Moreover, carbon nanofibers showed a high quantity of residual metal related to their synthesis. However, after graphitization, no metal residue was observed in the XRD spectra (Figure 2 and S1). The corresponding values for all the parameters obtained through XRD are shown in Table 1 using the peak (002) of carbon in all the different samples.

Table 1. Different Parameters Obtained from XRD for ^{12}C-CNF, ^{12}C-GCNF, ^{13}C-CNF, and ^{13}C-GCNF

sample	2θ (deg)	d (Å)	G (%)
^{12}C-CNF	26.40940	3.37082	82.73
^{12}C-GCNF	26.42480	3.36889	84.50
^{13}C-CNF	26.29798	3.38485	69.86
^{13}C-GCNF	26.35370	3.37782	76.31

TGAs performed in air atmosphere are shown in Figure 3 and Figure S2 for ^{13}C and ^{12}C fibers, respectively. As expected,

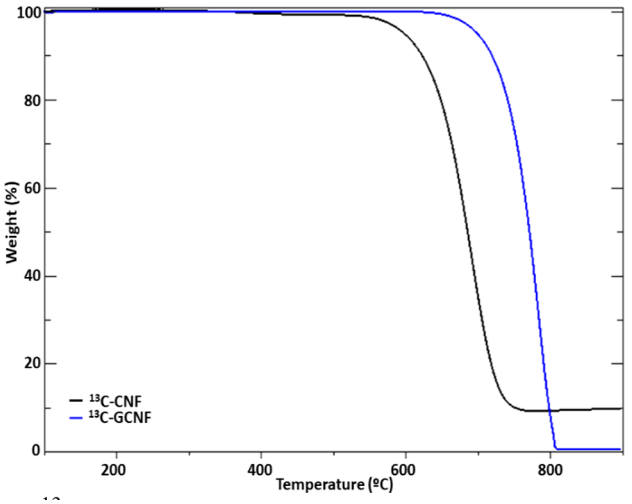

Figure 3. TGA of ^{13}C non-graphitized and graphitized carbon nanofibers.

higher thermal stability is observed for graphitized samples (779.93 °C for ^{12}C-GCNF, 773.21 °C for ^{13}C-GCNF) in comparison to pristine nanofibers (683.95 °C for ^{12}C-CNF, 683.52 °C for ^{13}C-CNF), corroborating the higher crystallinity in graphitized samples. Moreover, a total weight loss is observed for graphitized samples at 800 °C, while a residual (metallic) mass remains in the non-graphitized fibers (14.12% for ^{12}C-CNF, 9.31% for ^{13}C-CNF), which indicates the complete removal of all the catalytic nanoparticles in the graphitized nanofibers.

X-ray photoelectron spectroscopy (XPS) was also used to evaluate the type and abundance of oxygen groups in the samples (Figure S3a for ^{12}C and Figure S3b for ^{13}C). The C 1s and O 1s core-level spectra were fitted with Gaussian−Lorentzian (90G/10L) peaks to give separate main components.

The components of C 1s at different binding energies are 284.5 eV (sp^2 carbon bonds), 286.4 eV (sp^3, C−O−C bond), 287.8 eV (C═O bonds), 289.3 eV (C(O)O bonds),[45] and 291.4 eV ($\pi-\pi^*$ satellite),[46] this last one observed in graphitized nanofibers.

https://doi.org/10.1021/acsnano.2c09799
ACS Nano 2023, 17, 606−620

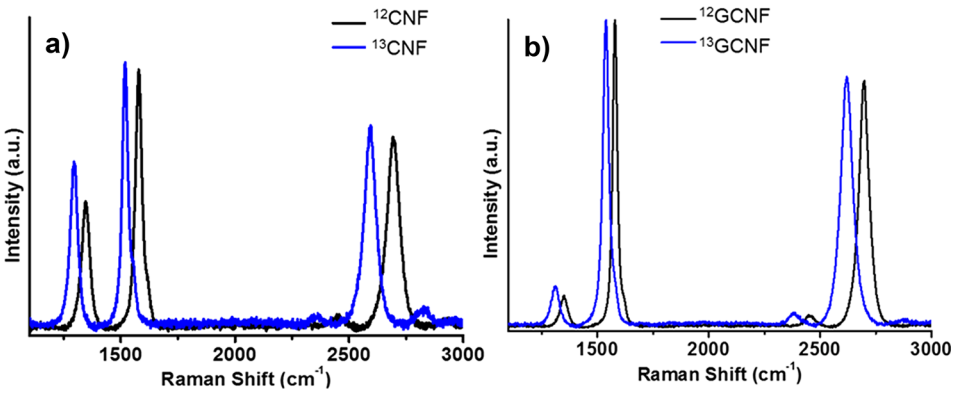

Figure 4. Raman spectra of ^{12}C and ^{13}C of (a) non-graphitized and (b) graphitized carbon nanofibers.

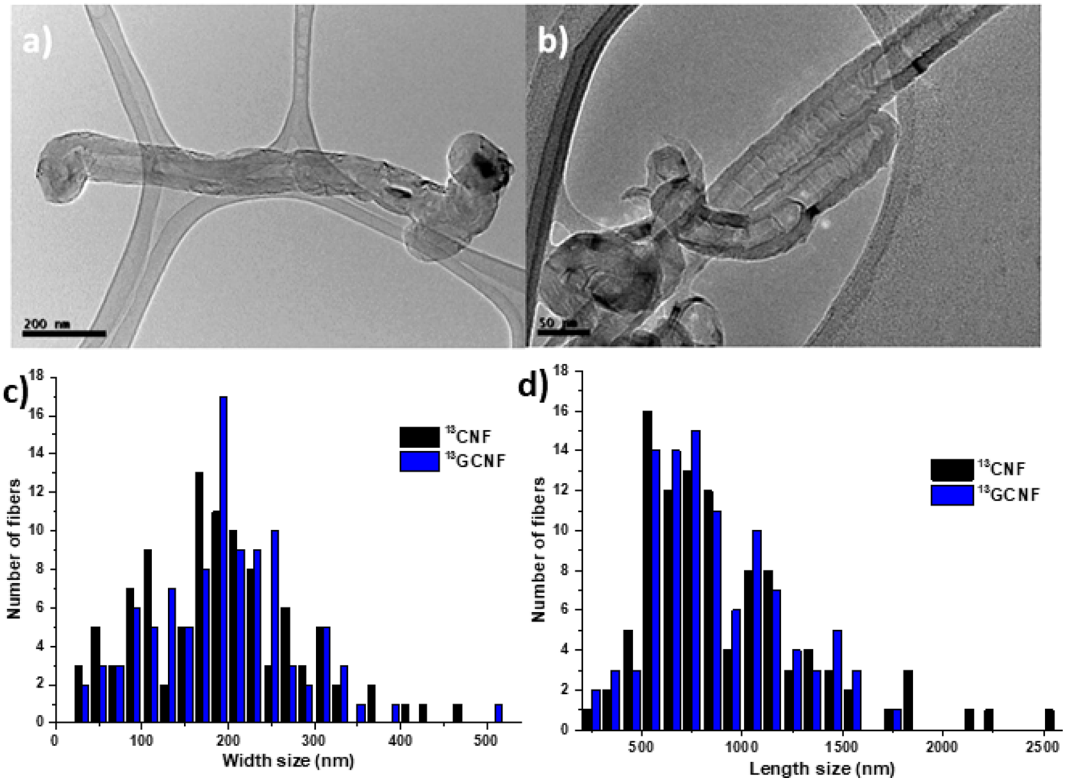

Figure 5. TEM images of (a) ^{13}C non-graphitized and (b) graphitized nanofibers. Distributions of (c) diameters (width) and (d) length size of ^{13}C carbon nanofibers.

On the other hand, the deconvolution of O 1s spectra produces three main peaks in non-graphitized fibers. These peaks at around 531.08 and 532.03 eV are generally assigned to C═O (in either carbonyl or carboxyl groups),[47] and that at 533.43 eV to C−O (singly bonded oxygen).[48] The graphitization produces in general a reduction in the oxygen content, mainly visible in the C═O peaks.

The increase in intensity of the $\pi \rightarrow \pi^*$ shake-up satellite band of graphitic carbon (Figure S4) observed between non-graphitized and graphitized ^{12}C and ^{13}C carbon nanofibers is due the reduction of defects in the material after removal of oxygen atoms.[49]

^{12}C-CNF and ^{13}C-CNF were also analyzed by Raman spectroscopy (Figure 4), where three bands are observed, corresponding to D, G, and 2D bands. The introduction of heavier ^{13}C atoms into the structure leads to downshifts in all the Raman modes. The magnitude of these downshifts depends on the frequency of the mode: those at higher frequencies shift more than modes at lower frequencies, as described by the simple harmonic oscillator model.[33,50,51]

For this reason it is possible to quantify the percentage of enrichment of ^{13}C of our sample, following the next equation:[52,53]

$$\frac{(\omega_0 - \omega)}{\omega_0} = 1 - \sqrt{\frac{12 + c_0}{12 + c}} \tag{2}$$

where ω_0 is the frequency of the ^{12}C sample, ω corresponds to the frequency of the ^{13}C sample, c corresponds to the concentration of ^{13}C in the enriched sample, and $c_0 = 0.0107$ is the natural abundance of ^{13}C.

After applying this equation, we find that before graphitization carbon nanofibers ^{13}C-CNF have an enrichment of 95.48 wt% (1519.89 cm^{-1}). After graphitization, this value

https://doi.org/10.1021/acsnano.2c09799
ACS Nano 2023, 17, 606−620

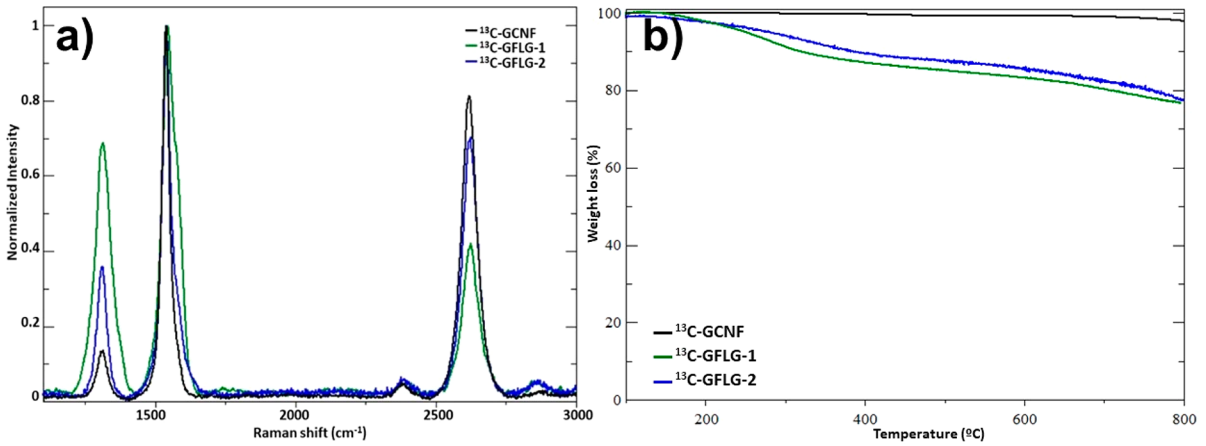

Figure 6. (a) Raman spectra and (b) TGA of carbon nanofibers using graphitized carbon nanofibers and melamine or glucose as exfoliants (^{13}C-GFLG-1 and ^{13}C-GFLG-2, respectively).

decreases to 65.10 wt% (1538.56 cm^{-1}) for ^{13}C-GCNF. These data agree with the results of elemental analysis quantifying ^{12}C with 2.82 and 33.12 wt% for ^{13}C-CNF and ^{13}C-GCNF, respectively. The reason for this exchange in the $^{13}C/^{12}C$ ratio is not clear yet and is currently under investigation in our groups. Different graphitization conditions might also be employed to avoid the dilution in ^{13}C content.[54]

Raman spectroscopy allows us to study the degree of crystallization and graphitization in carbon structures through the relation between the intensities of the D (I_D), G (I_G), and 2D (I_{2D}) bands.[55,56] The lower value of the ratio between I_D and I_G intensities after the graphitization process (around 0.10−0.14 for both samples, Table 1) indicates the loss of defects and the increase in the crystallization of the carbon nanofibers.

The percentage of ^{12}C in the ^{12}C samples observed by elemental analysis was 87.20 wt% for the pristine fibers (^{12}C-CNF) and 98.79 wt% for the graphitized ones (^{12}C-GCNF), which confirms once more the high quality of the graphitized fibers. Meanwhile, the percentages of H, N, and S are similar in both non-graphitized (0.14 wt% of H, 0.03 wt% for N, and 0.03 wt% for S) and graphitized carbon nanofibers (0.01 wt% of H, 0.02 wt% for N, and 0.02 wt% for S). For ^{13}C samples, similar results and percentages of the elements in the samples were found in ^{13}C-CNF (0.12 wt% of H, 0.04 wt% for N, and 0.03 wt% for S) and ^{13}C-GCNF (0.01 wt% of H, 0.03 wt% for N, and 0.02 wt% for S).

Finally, Figure 5 and Figure S5 show typical TEM images for graphitized and non-graphitized carbon nanofibers, which have homogeneous structure and uniform diameter of around 180 nm with lengths about 800 nm.

All the characterization techniques led us to conclude that both ^{12}C and ^{13}C fibers show similar structures. Pure graphitized samples exhibit an improvement in their thermal properties, due to a higher degree of crystallinity and to the absence of catalytic nanoparticles.

Synthesis of Few-Layer Graphene. The exfoliation of carbon nanofibers was performed by using two exfoliating agents, melamine and glucose, through a ball milling treatment for the synthesis of FLG.[36,57,58] The advantage of using a ball milling treatment is that, by changing the exfoliating agent and the milling parameters, there is the possibility of obtaining graphene flakes with different sizes and of tuning the C/O ratios.[36,39] Moreover, the process can be considered a green protocol because the exfoliating agent can be recycled and reused in different treatments.

In a typical experiment, the carbon nanofibers and the exfoliating agent are introduced in a stainless-steel grinding bowl with 10 stainless-steel balls (1 cm diameter), and the mechanochemical treatment is performed in a Resch ball mill at room temperature and pressure conditions. After the treatment, the solid is suspended in 20 mL of deionized water, sonicated for 1 min, and then dialyzed to remove the exfoliating agent. The final dispersion is stored for 5 days to allow the remaining carbon fibers to separate from the graphene sample. Finally, the resulting supernatant is separated and lyophilized at −80 °C with a pressure of 0.005 bar to obtain FLG powder.

All the results of the exfoliation of the carbon nanofibers were analyzed mainly by Raman spectroscopy to characterize the quality of the flakes, although the final yield of the process was also considered (Figure S6, Table S2).

In the Raman spectra, there are three principal bands useful to characterize graphene materials: D, G, and 2D bands. The D band is related to the presence of defects, whereas the G band represents the degree of graphitization; therefore, the intensity ratio between these two bands (I_D/I_G) can serve to quantify the density of defects in the graphene material.[59] Finally, the 2D band can be used to determine the number of layers through its full width at half-maximum (FWHM[60])—a narrow 2D band indicates a low number of layers.[61]

Considering the information obtained from the Raman spectra and the final yield of graphene obtained, we established a milling time of 2 h at 100 rpm and 5 h at 250 rpm when using melamine and glucose, respectively, as exfoliating agents.

Figure 6 shows the Raman spectra and the TGA of the graphene materials prepared under the optimized conditions, starting with the ^{13}C-GCNF (see Figure S7 for ^{12}C materials). As already described elsewhere,[36,58] the ratio I_D/I_G in the spectra of the graphene materials is lower (Table 2) when using melamine as exfoliating agent in comparison to glucose, which indicates the presence of fewer defects in the former sample. This agrees with the TGA results.

Figure 7 shows a comparison between the Raman spectra of the different fibers and FLG prepared using melamine with graphitized (^{13}C-GFLG-1) and non-graphitized (^{13}C-FLG-1) carbon nanofibers, where the shifts in the Raman bands depend on the percentage of ^{13}C as previously described

https://doi.org/10.1021/acsnano.2c09799
ACS Nano 2023, 17, 606−620

Table 2. Raman Spectroscopy Parameters (I_{2D}/I_G, I_D/I_G Bands, FWHM, and 2D and G Position Bands) of ^{12}C and ^{13}C Nanomaterials[a]

sample	I_D/I_G	I_{2D}/I_G	FWHM (cm^{-1})	2D position (cm^{-1})	G position (cm^{-1})
^{13}C-CNF	0.66	0.72	69.08	2593.78	1519.89
^{13}C-FLG-1	1.48	0.54	61.60	2586.60	1519.26
^{13}C-GCNF	0.14	0.80	68.22	2619.20	1538.56
^{13}C-GFLG-1	0.70	0.42	63.77	2622.70	1545.98
^{13}C-GFLG-2	0.36	0.81	63.76	2619.02	1539.80
^{13}C-GGO	0.86	0.09	–	2634.67	1565.34
^{12}C-CNF	0.50	0.76	71.10	2693.80	1578.50
^{12}C-GCNF	0.10	0.78	62.91	2696.88	1579.04
^{12}C-GFLG-1	1.33	0.57	69.43	2697.74	1583.88
^{12}C-GFLG-2	0.55	0.67	62.49	2699.91	1581.54
^{12}C-GGO	0.82	0.12	–	2677.62	1584.85

[a]Samples were carbon nanofibers and graphitized carbon nanofibers (^{12}C-CNF, ^{12}C-GCNF, ^{13}C-CNF, and ^{13}C-GCNF), FLG prepared by exfoliation of carbon nanofibers using glucose (^{13}C-FLG-1, ^{12}C-GFLG-1, and ^{13}C-GFLG-1) or melamine (^{12}C-FLG-2 and ^{13}C-GFLG-2) as exfoliating agent, and graphene oxide prepared from graphitized carbon nanofibers (^{12}C-GGO and ^{13}C-GGO).

(Figure 7a and data in Table 2). Also, in Table 2, we observe the relationship between the different bands I_{2D}/I_G, I_D/I_G and the FWHM for the different ^{13}C nanomaterials. It is important to mention that the percentage of ^{13}C in FLG is 95.48 wt% for ^{13}C-FLG and 65.10 wt% for ^{13}C-GFLG (the same value as the starting fibers). Only CVD graphene grown on a substrate has been described in the literature with such a high ^{13}C percentage.[26,28−30,32−34,50,62] Other papers describe the synthesis of GO in which the amount of ^{13}C is only around 7%.[35] Our values are much higher in comparison to the data found in the literature for ^{13}C-graphene materials prepared on a mg scale, and it is also important to note the high yield in which the material is obtained along with the possibility of recycling the non-exfoliated fibers to produce other batches of ^{13}C-FLG.

Raman spectra were used to analyze the different characteristics of the ^{13}C-graphene materials (Figure S7a for ^{12}C and Table 2). In general terms, all the experiments related to the exfoliation of graphitized carbon nanofibers have shown a small width of FWHM in the 2D band and a I_{2D}/I_G ratio lower than 1, which corresponds to FLG. As already commented, lower values of I_D/I_G are observed when using melamine as exfoliating agent, indicating a less defective graphene in the case of melamine.[36,39] However, it should be emphasized that the exfoliation with glucose offers the advantage of using a non-toxic and environmentally friendly agent.

TGA was used to check the thermal stability of all samples of graphene (Figure 6 and Figure S7b for ^{12}C) under a nitrogen atmosphere. ^{12}C-GFLG and ^{13}C-GFLG show similar behaviors, with a residual loss of 1.8 and 1.9 wt%, respectively. However, the graphene obtained by exfoliation with melamine has a higher thermal stability in comparison with the graphene obtained using glucose as exfoliant agent, ^{13}C-GFLG-2 (11.9 wt%) and ^{12}C-GFLG-2 (14.4 wt%) in comparison with glucose samples ^{13}C-GFLG-1 (21.9 wt%) and ^{12}C-GFLG-1 (17.2 wt %). This confirms the less defective nature of FLG prepared using melamine as exfoliating agent. All these values are due to pyrolysis of the residual oxygen groups on the graphene surface.[63]

TEM images and size distributions of graphene obtained by the two methods of exfoliation are shown in Figure 8 for ^{13}C and Figure S8 for ^{12}C. The size distributions of ^{12}C and ^{13}C materials are very similar and mainly depend on the exfoliating conditions, larger flakes being observed when using melamine as exfoliating agent.

Although the yield of the preparation of FLG, considering the recovery of the non-exfoliated fibers, is quite high (around 44%), we have also exploited the possibility of resubmitting these fibers to a new exfoliation process. Figure 9 shows the characterization of the FLG materials when using glucose and melamine as exfoliating agents in a second exfoliation procedure, ^{13}C-GFLG-1-remain and ^{13}C-GFLG-2-remain, respectively. In general, we found smaller flakes, but the

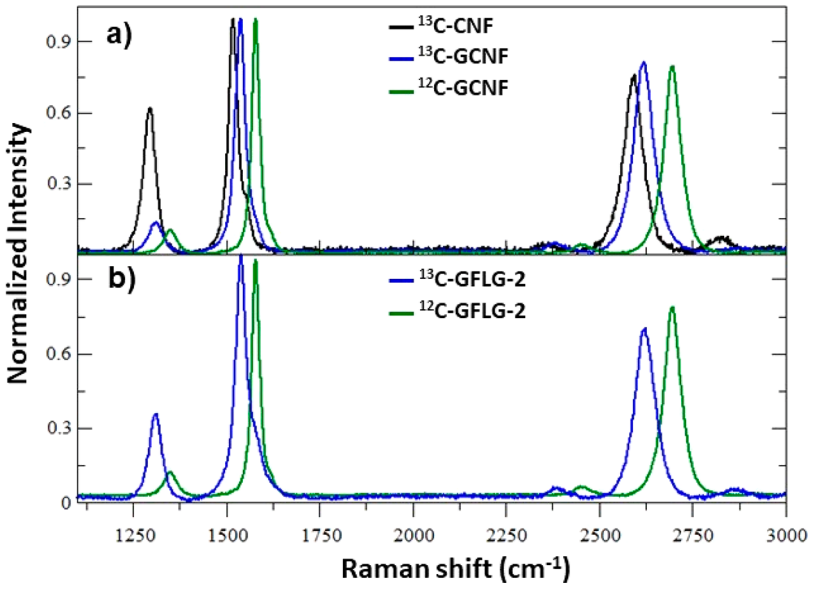

Figure 7. Comparison of Raman spectra of ^{13}C and ^{12}C nanomaterials: (a) carbon nanofiber and graphitized carbon nanofibers (^{13}C-CNF, ^{13}C-GCNF, and ^{12}C-GCNF) and (b) FLG prepared by exfoliation of carbon nanofibers and graphitized carbon nanofibers using melamine (^{13}C-GFLG-2 and ^{12}C-GFLG-2).

https://doi.org/10.1021/acsnano.2c09799
ACS Nano 2023, 17, 606−620

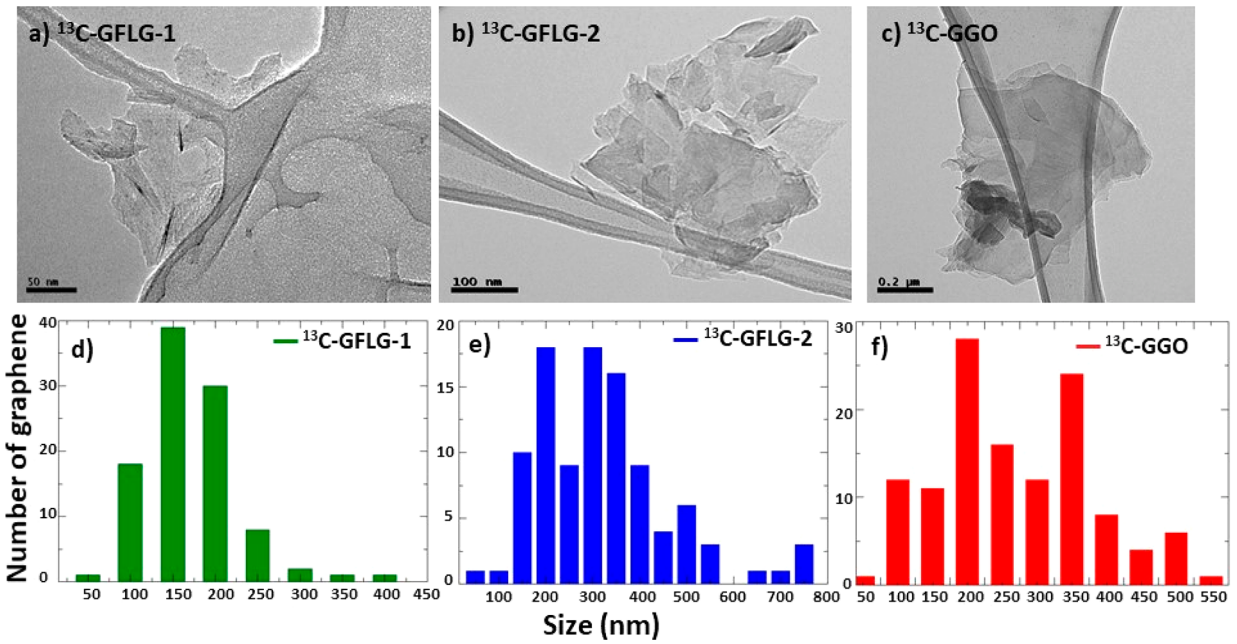

Figure 8. TEM images and size distribution of graphene obtained by exfoliation of the ^{13}C graphitized carbon nanofibers: (a, d) ^{13}C-GFLG-1, (b, e) ^{13}C-GFLG-2, and (c, f) ^{13}C-GGO.

TGA shows a similar thermal stability compared to the previous results of FLG, which corroborates the absence of oxidation during the treatment. Moreover, in Raman spectra, it is possible to observe an increase in the I_D/I_G ratio that is related to the decrease in the flake sizes.

Synthesis of Graphene Oxide. GO was prepared using a modified Hummers method starting from ^{12}C-GCNF or ^{13}C-GCNF as starting material[64] (see Methods).

Raman spectroscopy was used to follow the process from graphitized carbon nanofibers to graphene oxide, where it is possible to observe the disappearance of the 2D band in the graphene oxide prepared from graphitized carbon (GGO) for both samples (Figure 10a for ^{13}C, Figure S9a for ^{12}C, and Table 1), due to loss of interlayer bonding of graphene layers.[65] It is also possible to observe, for both samples ^{12}C and ^{13}C, an increase in the D band correlated with the appearance of defects in the structure.

Figure 10b for ^{13}C and Figure S9b for ^{12}C were used to observe the thermal stability of the GO nanomaterial in a nitrogen atmosphere. In general, TGA analysis shows a low percentage of oxygen groups on the surface compared to other typical GO syntheses, revealing a 31.2% weight loss for ^{13}C-GGO.

TEM image and size distribution of graphene oxide are shown in Figure 8 and Figure S8. The medium lateral size is around 220 nm for ^{12}C-GGO (Figure S8) and about 240 nm for ^{13}C-GGO (Figure 8), again corroborating similar materials from ^{12}C and ^{13}C fibers.

Finally, the colloidal stability of the ^{13}C and ^{12}C materials in deionized water was evaluated by UV−vis absorption spectroscopy (Figure S10) at 660 nm for FLG and 386 nm for GO.[40] Nanomaterial powders were re-dispersed at three different concentrations (0.2, 0.1, and 0.05 mg/mL). The stability of FLG (^{12}C-GFLG-1, ^{13}C-GFLG-1) increases significantly with respect to that of graphitized carbon nanofibers (^{12}C-GCNF, ^{13}C-GCNF). Moreover, the stability of graphene oxide (^{13}C-GGO, ^{12}C-GGO) was compared to that of a commercial source (GO-Antolin). In all the experiments, it is possible to observe a high stability of our ^{13}C nanomaterials, which show a minor sedimentation after 48 h (around 25% and 22.5% for ^{13}C-GGO and ^{13}C-GCNF-1, respectively). Another great advantage of this methodology is the use of glucose as exfoliating agent, which makes the material prepared with the present protocol ideal for biological experiments and applications.

Solid-State ^{13}C Magic-Angle-Spinning Nuclear Magnetic Resonance Spectroscopy (^{13}C MAS NMR). Finally, high-resolution solid-state NMR spectroscopy combined with magic angle spinning (MAS) has been used to characterize ^{13}C-GGO and ^{13}C GFLG-1, based on the work from Bianco et al.,[66,67] where MAS NMR played a key role for a comprehensive characterization of functionalized graphene derivatives. The enrichment of graphene with ^{13}C enables the structural characterization in shorter times in comparison to the non-labeled sample, where the NMR-active carbon isotope (^{13}C) is present naturally at only 1.1%. Figure 11, left, shows the MAS NMR spectrum of ^{13}C-GGO, where two peaks are observed. The signal at 168.4 ppm is attributed to the carbonyl ^{13}C═O species existing in GO, in agreement with theory and previously reported data, where a peak at 169 ppm was observed.[23,68,69] The peak centered at 130.0 ppm can be attributed to the aromatic carbon atoms of GO and possibly aromatic C-OH (phenol and/or aromatic diol species) according to previous peak assignment, reported at 129 ppm.[23,68−70] The absence of peaks at around 60−70 ppm indicates the minor presence of C-OH and epoxy groups attached to aliphatic carbons.[70] The absence of these aliphatic peaks in the MAS NMR spectrum is in good agreement with the TGA spectrum, which shows the low oxidation degree of this sample (Figure 10b). On the other hand, CP-MAS NMR spectroscopy was also carried out on the ^{13}C GFLG-1 sample. The sample could be tuned properly because it is a graphitized sample (absence of metals) in contrast to other works, where electric conductivity caused tuning problems.[67] The spectrum

https://doi.org/10.1021/acsnano.2c09799
ACS Nano 2023, 17, 606−620

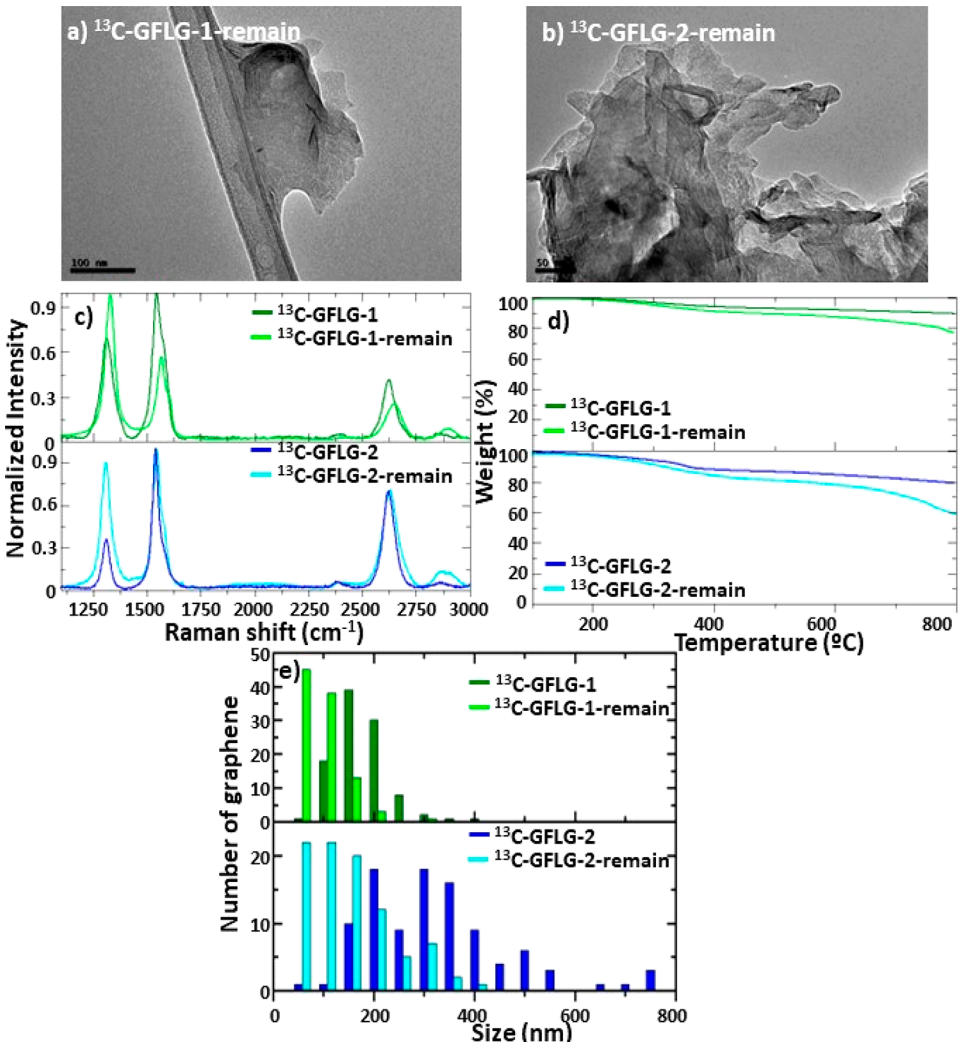

Figure 9. Comparison of characterization results obtained for FLG materials prepared from pristine graphitized carbon fibers (^{13}C-GFLG-1 and ^{13}C-GFLG-2) and recovered graphitized carbon fibers (^{13}C-GFLG-1-remain and ^{13}C-GFLG-2-remain): (a, b) TEM images, (c) Raman spectra, (d) TGA, and (e) size distribution of FLG flakes.

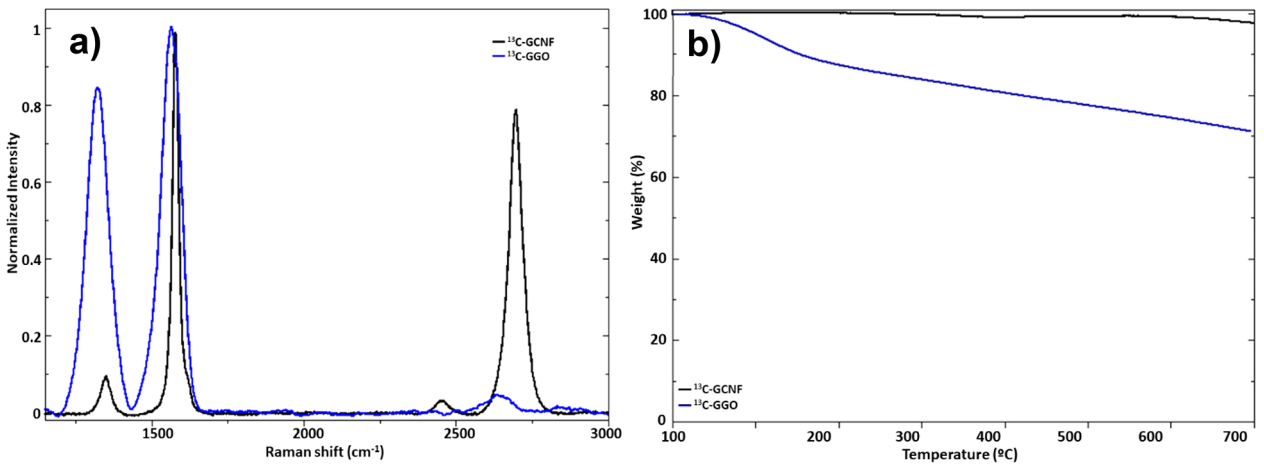

Figure 10. (a) Raman spectroscopy and (b) TGA of ^{13}C-graphene oxide (^{13}C-GGO).

for ^{13}C GFLG-1 shows a single and broad peak at 102.0 ppm that corresponds to sp^2-^{13}C from aromatic entities and conjugated double bonds (Figure 11, right). Due to the lack of functionalization, no other peaks are expected.

The shift to lower chemical shifts (101.5 ppm) compared to GO (130.0 ppm) can be explained due to the absence of oxygen in the ^{13}C-sp^2 surroundings or to magnetic susceptibility effects, knight shift effects, and/or other effects, as previously reported by Bianco et al.[67] It is consistent with

https://doi.org/10.1021/acsnano.2c09799
ACS Nano 2023, 17, 606−620

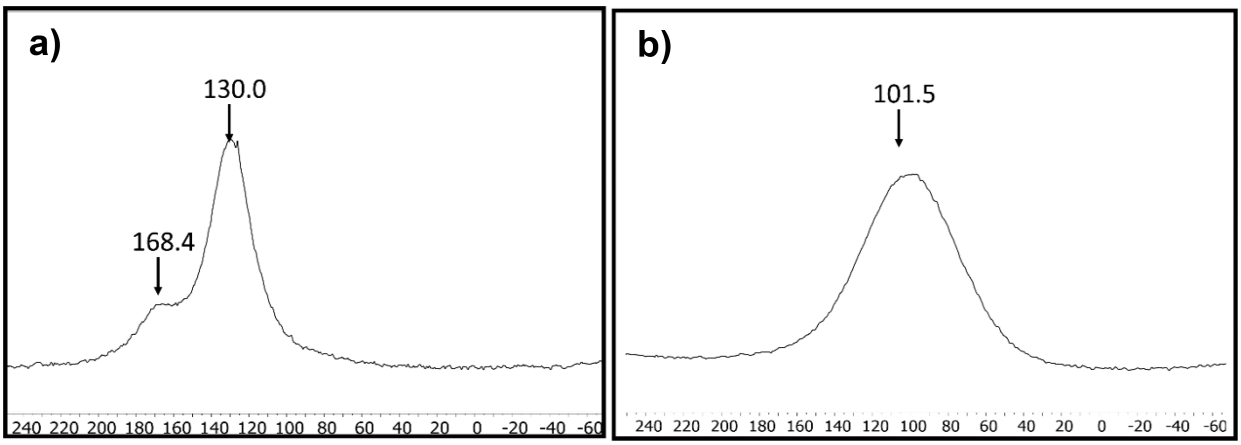

Figure 11. MAS ^{13}C NMR spectra for (a) ^{13}C-GGO and (b) ^{13}C-GFLG-1.

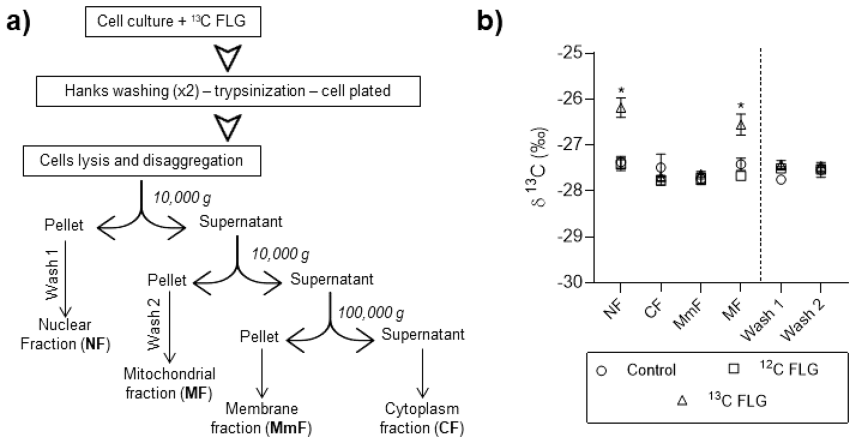

Figure 12. (a) Subcellular fractionation at serial centrifugation steps and (b) their comparison.

Table 3. δ^{13}C Values (‰, with SD in Parentheses) and %C of the Different Subcellular Fractions

sample		trypsin	NF	wash 1	MF	wash 2	CF	MmF
control	δ^{13}C	−22.75	−27.37	−27.75	−27.42	−27.54	−27.49	−27.73
		(0.033)	(0.090)	(0.02)	(0.095)	(0.115)	(0.205)	(0.080)
	%C	17.45	38.43	38.63	38.37	39.48	38.48	38.75
^{12}C-GFLG-1	δ^{13}C	−22.77	−27.42	−27.50	−27.67	−27.53	−27.77	−27.73
		(0.175)	(0.095)	(0.025)	(0.05)	(0.040)	(0.075)	(0.09)
	%C	17.80	38.14	40.76	38.56	38.40	38.07	38.75
^{13}C-GFLG-1	δ^{13}C	−13.39	−26.18	−27.42	−26.55	−27.45	−27.69	−27.63
		(0.057)	(0.150)	(0.06)	(0.16)	(0.025)	(0.01)	(0.040)
	%C	16.04	38.87	39.08	38.41	38.09	38.81	38.37

the lower chemical shift values for ^{13}C-sp^2 carbon signals found for graphite nanofibers (^{13}C-sp^2 chemical shift of 80 ppm[71]) and graphite powder (^{13}C-sp^2 chemical shift of 97 ppm[72]) in comparison to oxidized graphene samples.

The bandwidths of the ^{13}C-sp^2 peaks for ^{13}C-GGO (10 400 Hz (26 ppm)) and for ^{13}C-GFLG-1 (26 000 Hz (65 ppm)) are common values observed for solid-state NMR due to chemical shift anisotropy and other factors.[67,71] As observed for graphite nanofibers (bandwidth of 90 ppm)[71] or graphite,[72] it can be related to the presence of different chemical species with different magnetic susceptibility (heterogeneity in the types of sp^2 carbons or many non-equivalent ^{13}C sites), or due to structural heterogeneity, which could include sheet stacking that could modulate chemical shifts, or even due to the presence of conduction electrons. Notably, the presence of adjacent ^{13}C atoms (all at high abundance) also contributes to peak broadening because of their spin−spin couplings.

Proof of Concept: Detection of Graphene in Subcellular Organelles. Stable isotope labeling of materials is a relevant method to evaluate their environmental impact or their degradation (biostimulation, bioaugmentation, etc.[73]). However, as far as we know, no study has described the distribution, detection, and quantification of graphene materials inside the different cellular compartments. In the present work, our ^{13}C-graphene material is suitable to trace graphene derivatives assimilated by cells, even at very low

https://doi.org/10.1021/acsnano.2c09799
ACS Nano 2023, 17, 606−620

concentrations. For this purpose, HepG2 cells were exposed to a dispersion of ^{13}C- and ^{12}C-FLG derivatives (10 μg/mL). In order to avoid any effect produced by metal or melamine traces, graphitized FLG samples prepared using glucose as exfoliating agent were used (GFLG-1), even though these materials present a lower percentage of ^{13}C (63 vs 95%).

After 7 days of incubation, a subcellular fractionation was performed by means of serial centrifugation steps (Figure 12a). We were able to separate fractions including the nucleus (NF), cytoplasm (CF), membranes (MmF), and mitochondria (MF). To ensure that the FLG present in the medium does not contaminate the different fractions, the cells were washed twice, trypsinized, and seeded for 24 h before starting the fractionation process. Moreover, and to completely exclude the possible contamination of the subcellular fractions with graphene materials, for the control experiment, ^{13}C-GFLG-1 was added to untreated cells immediately before the fractionation process.

The extracted fractions were lyophilized and analyzed by IRMS. ^{13}C NMR spectroscopy was not employed for the analysis mainly because of the presence of an excess (with respect to graphene) of organic material in the sample that also contains ^{13}C (as natural abundance) and, therefore, would also give ^{13}C NMR signals in the spectrum that could overlap with the ^{13}C-graphene peaks. The results are given in the form of stable carbon isotope ratios (δ^{13}C). δ^{13}C values of the different subcellular fractions can be found in Table 3, and they are plotted in Figure 12b for comparison. δ^{13}C values of cytoplasm and membrane fractions were similar in all cases, while nuclear and mitochondrial fractions of cells treated with ^{13}C-GFLG-1 were enriched in ^{13}C by around 1‰ relative to both control and ^{12}C-GFLG-1-treated cells. It is important to note that values found in the buffer obtained from the washing steps of nuclear and mitochondrial fractions (wash 1 and wash 2, respectively) were similar in all the cases, which excludes contamination. Additionally, plasma membrane fractions, extracted in the trypsin part, present an enormous increase in ^{13}C (Table 3), corroborating the fact that graphene materials in the culture media and those attached to the plasma membrane were removed from the cellular environment.

To quantify ^{13}C-FLG in nuclei and in mitochondrial fractions, δ^{13}C values were transformed into the amount of ^{13}C-FLG in the different organelle fractions ($m^{^{13}\text{C-FLG}}$) following eqs 1−3. The relation m_{dry}/m_{wet} was 0.1 for nuclei fractions and 0.09 for mitochondria ones, the weights of the lyophilized pellets being around 3 and 3.5 mg for nuclei and mitochondria fractions, respectively. Moreover, cells were treated with a concentration of 10 μg/mL with a total dose of 50 mg. With these data and using eq 4, it is possible to calculate that 4.1% of the applied dose can be found in the mitochondrial fraction, while 4.9% of the dose ends up in the nuclear fraction. The rest of the dose cannot enter the cell and remains in the plasma membrane or in the culture media. These studies and the possibility of detecting graphene derivatives within cellular compartments may help in studying the mechanisms of interaction of these materials at the cellular level. This approach may be relevant for the quantitative analysis of the internalization of glioblastoma multiforme (GBM). We have previously shown using confocal microscopy that GBM can reach mitochondria in epithelial cells.[74] Other authors mixed GO with FITC-labeled BSA prior to cells' incubation and then assayed internalization by confocal microscopy, combined with cell flow cytometry and TEM.[75] TEM has been widely used to evaluate the internalization of GBM in several biological models, in vitro and in vivo,[76−78] in some other instances combined with Raman spectroscopy.[79] However, all these approaches are qualitative and just allow one to determine the presence of the material inside the cell or to compare between different experimental conditions. Labeling GBM with ^{13}C offers the possibility to study biodistribution and bioaccumulation in vitro and in vivo in a more accurate way, allowing the correlation between the amount of graphene reaching cellular compartments with alterations in these compartments.

CONCLUSION

The synthesis of bulk quantities of ^{13}C-labeled graphene materials is important for basic studies. But especially the use of graphene in real-world applications makes it increasingly necessary to use methods for the detection of this material and its derivatives in natural matrices, which will favor its traceability and the development of safe and environmentally friendly systems. The present work contributes significantly to this target by describing the synthesis of graphene materials with varying degrees of oxidation and sizes, all enriched with high amounts of ^{13}C, that have not been described to date for bulk materials.

The approach is simple and easily scalable, enabling high yields so that materials can be prepared in high enough quantities to be used in a wide range of applications.

^{13}C labeling also enables graphene to be detected even after it has been modified or degraded, without the need for D- or G-band Raman detection or microscopy imaging analysis, so it could be used for degradation studies or even for developing occupational exposure limits.

The results suggest that the use of ^{13}C materials is a suitable method to assess the biodistribution of graphene in different models and organisms. To date, ^{14}C-graphene has been used for such studies, but although it is a valid approach, it generates a number of technical and practical issues due to radioactivity. With the use of ^{13}C-graphene, these problems would be avoided, generating an approach that is simpler and applicable in all types of environments. One of the main advantages of using ^{14}C is its quantification by imaging techniques. However, the use of MRSI is progressively gaining ground.[19−21] Combining this technique with the use of ^{13}C-graphene would enable real-time biodistribution studies in animal models.

^{13}C materials could also be used for bioaccumulation studies in different ecosystems. The use of ^{13}C-graphene allows for much simpler and less environmentally invasive experiments than the use of ^{14}C. Previous studies with ^{13}C-labeled toxic compounds demonstrate the feasibility and applicability of our proposal.[80]

METHODS

Materials. Unless otherwise noted, materials were purchased from Fluka, Aldrich, Acros, ABCR, Merck, and other commercial suppliers and used as received. $^{13}CH_4$ (99% ^{13}C) was purchased from SIAD (Società Italiana Acetilene Derivati S.p.A.)

Equipment. XRD spectra were recorded on a Philips (Panalytical) model using Cu Kα_1 (1.54056 Å) at 40 kV and 40 mA. Diffraction patterns were collected in a range of 10−90° 2θ.

Raman spectra were recorded on an InVia Renishaw instrument using powder samples with a 532 nm point-based laser with a power

https://doi.org/10.1021/acsnano.2c09799
ACS Nano 2023, 17, 606−620

density below 1 mW μm^{-2} to avoid laser heating effects. The resulting spectra (with around 30−40 random locations on each sample) were fitted with Lorentzian-shaped bands in each characteristic band of graphene (D, G, and 2D).

TGA was performed on a TA Instruments Q50 instrument at 10 °C min^{-1} under nitrogen or air flow, depending on the sample, from 100 to 800 °C.

TEM was performed on a JEOL 2100 high-resolution transmission electron microscope (HRTEM) at an accelerating voltage of 100 kV using stable dispersions of graphene dip-cast on Lacey copper grids (3.00 mm, 200 mesh), coated with carbon film, for further drying under vacuum.

UV−vis spectra were recorded on a Cary 5000 UV-vis-NIR spectrophotometer with 1 cm quartz cuvettes. Dual beam mode and baseline correction were used throughout the measurements of FLG (660 nm) and GO (386 nm) for 2−48 h at different time intervals. The determination of the concentration of graphene was determined from the optical absorption coefficient at maximum absorbance, using

$$A = \alpha \times l \times c \tag{3}$$

where l (m) is the light path length, c (g L^{-1}) is the concentration of our material of interest, and α (L g^{-1} m^{-1}) is the absorption coefficient, with α = 690 L g^{-1} m^{-1} at 660 nm for FLG and α = 1130 L g^{-1} m^{-1} at 386 nm for GO. The optical absorbance divided by cell length against the concentration exhibited Lambert−Beer behavior.

MAS NMR spectroscopy was performed in a Bruker AV400 wide-bore spectrometer operating in a 9.4 T magnetic field (^{13}C, 100.62 MHz) and equipped with a 2.5 mm diameter solid-state probe head. A multinuclear double-channel probe (BL2.5 170-$^{31}P/^{19}F$-^{1}H) with a spinning speed up to 35 kHz was employed. An amount of around 10 mg of sample was used for each material, ^{13}C-GGO and ^{13}C-GFLG-1. A pulse sequence of direct excitation on ^{13}C via ^{1}H decoupling was used. ^{13}C MAS NMR spectra of both materials were recorded with a spectral width of 496.9 ppm and an FID size of 2048, with 256 scans, an acquisition time of 0.02 s, a pulse width of 6.2 μs, and a long recycle delay of 180 s based on the previous work reported by Cai et al.[69] The spin rate for the ^{13}C MAS NMR experiment on ^{13}C-graphene oxide was 10 kHz and for ^{13}C-FLG was 20 kHz. MestReNova v.12.0 was used for data processing.

^{13}C Quantification by Elemental Analysis Coupled to Isotope Ratio Mass Spectrometry (EA-IRMS). Lyophilized subcellular fractions were used to detect ^{13}C- content by IRMS. Each sample was weighed with a precision balance MX5 (Metler, Toledo) and then encapsuled in tin capsules for isotope analysis. EA-IRMS analyses were performed using a Flash EA1112-ConFloIV analyzer with a MAS 200R carousel autosampler, and a Delta V Advantage (Thermo Scientifics, Bremen, Germany) IRMS was used as the detection system. The elemental analyzer also has a thermal conductivity detector (TCD) for elemental analysis. In the elemental analyzer, the samples pass through a combustion and reduction reactor at 1020 °C, transforming them into CO_2 and N_2 gases, which are separated in a chromatographic column at 45 °C. These gases are then transferred to the TCD and IRMS. The carrier gas (helium) was maintained during the analysis at 100 mL min^{-1} and the reference gases (CO_2 and N_2) at 250 mL/min. The reference gases were calibrated against internationally certified reference materials supplied by the International Atomic Energy Agency (IAEA). Certified reference materials (IAEA-N1, IAEA-N2, IAEA-CH6, NBS-22, USGS-40, and USGS-41) and laboratory standards were also introduced in each sample sequence.

Synthesis of Carbon Nanofibers. According to the optimized synthesis conditions, 10 mL of an aqueous solution containing 36.6 mg of $NiSO_4$ was slowly sprayed over four alumina plates (75 × 15 mm) heated at 200 °C in order to homogeneously cover their surfaces. $NiSO_4$ was sprayed over both sides of the alumina plates. For each batch of carbon nanofibers, 12 spayed alumina plates were placed inside the tubular reactor (inner diameter 45 mm) within a quartz holder properly designed to maximize the exposed area. The tubular reactor was placed within a furnace to homogeneously heat the materials. Prior to each treatment, air was purged from the reactor by an Ar flow (200 mL min^{-1}) for 30 min. Subsequently, the furnace was heated at 800 °C (10 °C min^{-1}) maintaining the Ar flow in the reactor. After the final temperature was stabilized for 15 min, the gas flow was switched to H_2 (140 mL min^{-1}) to completely reduce the Ni salt, forming Ni nanoparticles on the surface of the Al_2O_3 support. After reduction for 1 h, CH_4 (60 mL min^{-1}) was added to the H_2 flow, reaching a total flow of 200 mL min^{-1} and a linear velocity of ∼12.6 cm min^{-1}. The H_2/CH_4 mixture was flowed within the reactor for 8 h in order to grow the carbon nanofibers. Then, the furnace was purged by an Ar flow (200 mL min^{-1}) for 15 min and cooled. To avoid oxidation and/or partial degradation of the products by accidental exposure to air, the reactor was left to stabilize at room temperature overnight before being opened to remove the Al_2O_3 plates with the carbon nanofibers grown on them. The carbon nanofibers were detached from the alumina plates by sonication in EtOH 96% for 1 h and subsequently collected by centrifugation at 4500 rpm for 30 min. Then, the fibers were suspended in aqueous HCl 5% for 24 h, in order to remove the accessible Ni nanoparticles, and washed twice with EtOH 96%. Finally, the material was dried at 60 °C overnight.

The preparation of ^{13}C-based carbon nanofibers was performed following the same procedure but replacing CH_4 with $^{13}CH_4$.

Synthesis of Few-Layer Graphene. Different milling parameters (time and rpm) were used to determine the best conditions of exfoliation of the carbon fibers, using ^{12}C-CNF as a model for further implementation with ^{13}C nanofibers (see Table S1).

Synthesis of Graphene Oxide. Graphene oxide was prepared using graphitized carbon nanofibers as starting material. 1 mg of ^{13}C-GCNF or ^{12}C-GCNF, 1 mL of H_2SO_4, and 1 mg $KMnO_4$ was stirred for 1 h at room temperature and 6 h at 70 °C. After this time, the material was washed with water until getting a neutral pH.

Subcellular Fractionation. HepG2 cells were plated into T25 flaks and incubated for 7 d with 10 μg mL^{-1} of ^{13}C- or ^{12}C-few-layer-graphene materials (^{12}C-GFLG-1 and ^{13}C-GFLG-1). Then, to ensure the full removal of adsorbed graphene materials, cells were washed with Hanks solution, detached with trypsin, and plated again into T25 flasks for another 24 h. After this time, cells were scraped and lysed using 500 μL of a pH 7.4 fractionation buffer (250 mM sucrose, 20 mM Hepes, 10 mM KCl, 1.5 mM $MgCl_2$, 1 mM EDTA, 1 mM EGTA, 1 mM dithiothreitol) supplemented with 1% protease inhibitor cocktail. Lysate was passed through a 25-Ga needle 10 times using a 1 mL syringe and incubated on ice for 20 min. Lysates were centrifuged at 720g for 5 min, obtaining the nuclear and cytoplasm/membrane fractions (pellet and supernatant, respectively). The nuclear fraction (NF; pellets) was washed by adding 500 μL of fractionation buffer, resuspended with a pipet, passed through a 25-Ga needle 10×, and then centrifuged again at 720g for 10 min. Buffer was removed (wash 1) and NF pellets were resuspended in fractionation buffer. Supernatants were centrifuged at 10000g, obtaining the mitochondrial (MF) and cytoplasm/membrane fraction (pellet and supernatant, respectively). MF was washed by adding 500 μL of fractionation buffer, resuspended with a pipet, passed through a 25-Ga needle 10×, and then centrifuged again at 10000g for 10 min. Buffer was removed (wash 2) and the mitochondrial pellet was resuspended in fractionation buffer. Finally, the cytoplasm/membrane fraction was centrifuged at 100000g for 1 h. Supernatant corresponds to cytoplasm fraction. For membrane fraction, the pellet was washed by adding 400 μL of the fractionation buffer and then re-centrifuged for 45 min. All the fractions were freeze-dried using a Telstar Lyoquest.

As a control, to completely exclude the possible contamination of graphene materials between the subcellular fractions, ^{13}C-GFLG-1 was added to untreated cells immediately before the fractionation process (avoiding the incubation step).

Quantification of ^{13}C-Graphene Materials in Subcellular Organelles. To quantify the amount of graphene materials entering inside the different organelles, the extracted pellets were lyophilized to obtain a dry powder. The samples were analyzed by IRMS, and the results were provided as δ values (Table 3). The δ value was converted into a $^{13}C/^{12}C$ ratio (r) following eq 4, where the $(^{13}C/^{12}C)_{standard}$ was 0.0111802, the ratio of the Vienna Pee Dee

https://doi.org/10.1021/acsnano.2c09799
ACS Nano 2023, 17, 606−620

Belemnite (VPDB) standard sample.[25] ω^{13}_{C} (eq 5) is the percentage of ^{13}C in mass (total weight of ^{13}C atoms/total weight of carbon atoms); thus, $\omega^{13}_{C\ (organelle\ fraction)}$ is the percentage of ^{13}C in mass for the organelle fraction from cells exposed to ^{13}C-FLG, and $\omega^{13}_{C(control)}$ is the percentage of ^{13}C in mass for the organelle fraction from control cells. $\omega^{13}_{C\text{-}FLG}$ (the percentage of ^{13}C in mass in ^{13}C-FLG) was calculated from Raman data, obtaining a value of 68.5% for ^{13}C-GFLG-1.

$$r = \left(\frac{\delta}{1000} + 1\right) \times \left(\frac{^{13}C}{^{12}C}\right)_{standard} \quad (4)$$

$$\omega^{13}_{C} = \frac{r \times 13}{r \times 13 + 12} \times 100\% \quad (5)$$

The amount of ^{13}C-FLG in the different organelle fractions ($m^{13}_{C\text{-}FLG}$) can be calculated from eq 6, where ω_{carbon} is the content of carbon in each fraction obtained by IRMS (Table 2) and m_{wet} and m_{dry} are the weights of the organelle fractions before and after lyophilizing.

$$m^{13}_{C\text{-}FLG} = \frac{\left[\omega^{13}_{C(organelle\ fraction)} - \omega^{13}_{C(control)}\right] \times \left(\omega_{carbon} \times m_{organelle} \times \frac{m_{dry}}{m_{wet}}\right)}{\omega^{13}_{C\text{-}FLG}} \quad (6)$$

The content of ^{13}C-FLG in the different organelles was also expressed as percentage of applied dose (%ID, eq 7).

$$\%ID = \frac{m^{13}_{C\text{-}FLG}}{dose} \times 100\% \quad (7)$$

ASSOCIATED CONTENT

Supporting Information

The Supporting Information is available free of charge at https://pubs.acs.org/doi/10.1021/acsnano.2c09799.

Additional experimental details of the synthesis of graphene, including characterization by XRD, TGA, XPS, and TEM of carbon nanofibers; Raman, TGA, and TEM characterization of ^{12}C-graphene; and colloidal stability of the synthesized nanomaterials, including Figures S1−S10 and Tables S1 and S2 (PDF)

AUTHOR INFORMATION

Corresponding Authors

Maurizio Prato − *Department of Chemical and Pharmaceutical Sciences, INSTM UdR Trieste, University of Trieste, 34127 Trieste, Italy; Center for Cooperative Research in Biomaterials (CIC biomaGUNE), Basque Research and Technology Alliance (BRTA), 20014 Donostia San Sebastián, Spain; Basque Foundation for Science (IKERBASQUE), 48013 Bilbao, Spain;* orcid.org/0000-0002-8869-8612; Email: prato@units.it

Ester Vázquez − *Instituto Regional de Investigación Científica Aplicada (IRICA), Universidad de Castilla-La Mancha, 13071 Ciudad Real, Spain; Faculty of Chemical Science and Technology, Universidad de Castilla-La Mancha, 13071 Ciudad Real, Spain;* orcid.org/0000-0003-3223-8024; Email: ester.vazquez@uclm.es

Authors

Viviana González − *Instituto Regional de Investigación Científica Aplicada (IRICA), Universidad de Castilla-La Mancha, 13071 Ciudad Real, Spain*

Javier Frontiñan-Rubio − *Instituto Regional de Investigación Científica Aplicada (IRICA), Universidad de Castilla-La Mancha, 13071 Ciudad Real, Spain; Cell Biology Area, Department of Medical Sciences, Faculty of Medicine, Universidad de Castilla-La Mancha, 13071 Ciudad Real, Spain*

M. Victoria Gomez − *Instituto Regional de Investigación Científica Aplicada (IRICA), Universidad de Castilla-La Mancha, 13071 Ciudad Real, Spain; Faculty of Chemical Science and Technology, Universidad de Castilla-La Mancha, 13071 Ciudad Real, Spain;* orcid.org/0000-0002-3183-0504

Tiziano Montini − *Department of Chemical and Pharmaceutical Sciences, INSTM UdR Trieste, University of Trieste, 34127 Trieste, Italy; ICCOM-CNR, University of Trieste, 34127 Trieste, Italy;* orcid.org/0000-0001-9515-566X

Mario Durán-Prado − *Cell Biology Area, Department of Medical Sciences, Faculty of Medicine, Universidad de Castilla-La Mancha, 13071 Ciudad Real, Spain;* orcid.org/0000-0001-9652-5765

Paolo Fornasiero − *Department of Chemical and Pharmaceutical Sciences, INSTM UdR Trieste, University of Trieste, 34127 Trieste, Italy; ICCOM-CNR, University of Trieste, 34127 Trieste, Italy;* orcid.org/0000-0003-1082-9157

Complete contact information is available at: https://pubs.acs.org/10.1021/acsnano.2c09799

Author Contributions

V.G. synthesized and characterized FLG and GO. J.F.-R. performed the biological studies. T.M. synthesized carbon nanofibers. M.V.G. performed ^{13}C MAS NMR studies. E.V. designed the methodology and conceptualized the paper. V.G., E.V., J.F.-R., and M.P. wrote the paper. E.V., M.P., P.F., M.V.G., and M.D.-P. participated in analysis of the experimental data, interpretation, and correction of the paper. E.V. and M.P. conceived this work. All authors discussed the results, revised the final manuscript, and gave the final approval.

Notes

The authors declare no competing financial interest.

ACKNOWLEDGMENTS

This work was supported by the European Union Horizon 2020 research and innovation program Graphene Flagship under grant agreement core 3 (881603), the Spanish Ministerio de Economía y Competitividad, Project PDC2021-120735-I00 and FEDER-JCCM project UNCM13-1E-1663. We thank the services of the Instituto Regional de Investigación Científica Aplicada (IRICA). M.P. is the AXA Chair for Bionanotechnology (2016−2026). The authors gratefully acknowledge the financial support from the University of Trieste, INSTM and the Maria de Maeztu Units of Excellence Program from the Spanish State Research Agency (Grant No. MDM-2017-0720). We are grateful to Dr. Antonio Esaú Del Rio Castillo for initial exploration studies. César Merino is also acknowledged for technical support and productive discussions. M.V.G. thanks the Spanish Government (AEI/FEDER UE) for funding part of this work: Project PID2020-119636GB-I00, funded by MCIN/AEI/10.13039/501100011033 and CTQ2017-84825-R.

ABBREVIATIONS

FLG, Few-layer graphene; GO, Graphene oxide; GGO, Graphene oxide prepared from graphitized carbon; NMR, Nuclear magnetic resonance; TGA, Thermogravimetric analysis; XPS, X-ray photoelectron spectroscopy; XRD, X-ray powder diffraction; IRMS, Isotope ratio mass spectrometry; ICP-MS, Inductively coupled plasma mass spectrometry; TEM, Transmission electron microscopy; MRSI, Magnetic resonance spectroscopic imaging; CVD, Chemical vapor deposition; FWHM, Full width at half-maximum; NF, Nucleus; CF, Cytoplasm; MmF, Membranes; MF, Mitochondria; MAS NMR, Magic Angle Spinning Nuclear Magnetic Resonance; TCD, Thermal conductivity detector; VPDB, Vienna Pee Dee Belemnite

REFERENCES

(1) Ferrari, A. C.; Bonaccorso, F.; Fal'ko, V.; Novoselov, K. S.; Roche, S.; Boggild, P.; Borini, S.; Koppens, F. H.; Palermo, V.; Pugno, N.; Garrido, J. A.; Sordan, R.; Bianco, A.; Ballerini, L.; Prato, M.; Lidorikis, E.; Kivioja, J.; Marinelli, C.; Ryhanen, T.; Morpurgo, A.; et al. Science and technology roadmap for graphene, related two-dimensional crystals, and hybrid systems. *Nanoscale* **2015**, *7* (11), 4598−810.

(2) Johnson, K. K.; Koshy, P.; Yang, J. L.; Sorrell, C. C. Preclinical Cancer Theranostics—From Nanomaterials to Clinic: The Missing Link. *Adv. Funct. Mater.* **2021**, *31* (43), 2104199.

(3) Guo, M.; Zhao, L.; Liu, J.; Wang, X.; Yao, H.; Chang, X.; Liu, Y.; Liu, J.; You, M.; Ren, J.; Wang, F.; Wang, L.; Wang, Y.; Liu, H.; Li, Y.; Zhao, Y.; Cai, R.; Chen, C. The Underlying Function and Structural Organization of the Intracellular Protein Corona on Graphdiyne Oxide Nanosheet for Local Immunomodulation. *Nano Lett.* **2021**, *21* (14), 6005−6013.

(4) Fadeel, B.; Bussy, C.; Merino, S.; Vazquez, E.; Flahaut, E.; Mouchet, F.; Evariste, L.; Gauthier, L.; Koivisto, A. J.; Vogel, U.; Martin, C.; Delogu, L. G.; Buerki-Thurnherr, T.; Wick, P.; Beloin-Saint-Pierre, D.; Hischier, R.; Pelin, M.; Candotto Carniel, F.; Tretiach, M.; Cesca, F.; et al. Safety Assessment of Graphene-Based Materials: Focus on Human Health and the Environment. *ACS Nano* **2018**, *12* (11), 10582−10620.

(5) Loven, K.; Franzen, S. M.; Isaxon, C.; Messing, M. E.; Martinsson, J.; Gudmundsson, A.; Pagels, J.; Hedmer, M.; et al. NanoLund, Emissions and exposures of graphene nanomaterials, titanium dioxide nanofibers, and nanoparticles during down-stream industrial handling. *J. Expo Sci. Environ. Epidemiol* **2021**, *31* (4), 736−752.

(6) Chang, X.-L.; Ruan, L.; Yang, S.-T.; Sun, B.; Guo, C.; Zhou, L.; Dong, J.; Yuan, H.; Xing, G.; Zhao, Y.; Yang, M. Quantification of carbon nanomaterials in vivo: direct stable isotope labeling on the skeleton of fullerene C60. *Environ. Sci.: Nano* **2014**, *1* (1), 64−70.

(7) Chen, L.; Wang, C.; Yang, S.; Guan, X.; Zhang, Q.; Shi, M.; Yang, S.-T.; Chen, C.; Chang, X.-L. Chemical reduction of graphene enhances in vivo translocation and photosynthetic inhibition in pea plants. *Environmental Science: Nano* **2019**, *6* (4), 1077−1088.

(8) Sun, Y.; Yang, Y.; Tou, F. Y.; Niu, Z. S.; Guo, X. P.; Liu, C.; Yan, J.; Wu, J. Y.; Xu, M.; Hou, L. J.; Liu, M. Extraction and quantification of metal-containing nanoparticles in marine shellfish based on single particle inductively coupled plasma-mass spectrometry technique. *J. Hazard Mater.* **2022**, *424* (Pt A), 127383.

(9) Goodwin, D. G., Jr.; Adeleye, A. S.; Sung, L.; Ho, K. T.; Burgess, R. M.; Petersen, E. J. Detection and Quantification of Graphene-Family Nanomaterials in the Environment. *Environ. Sci. Technol.* **2018**, *52* (8), 4491−4513.

(10) Firlar, E.; Ouy, M.; Covnot, L.; Xing, Y.; Lee, D.; Chan, A.; He, Y.; Song, B.; Afelik, S.; Wang, Y.; Shahbazian-Yassar, R.; Oberholzer, J.; Shokuhfar, T. In situ graphene liquid cell-transmission electron microscopy study of insulin secretion in pancreatic islet cells. *Int. J. Nanomedicine* **2019**, *14*, 371−382.

(11) Paillet, M.; Parret, R.; Sauvajol, J.-L.; Colomban, P. Graphene and related 2D materials: An overview of the Raman studies. *J. Raman Spectrosc.* **2018**, *49* (1), 8−12.

(12) Li, D.; Hu, X.; Zhang, S. Biodegradation of graphene-based nanomaterials in blood plasma affects their biocompatibility, drug delivery, targeted organs and antitumor ability. *Biomaterials* **2019**, *202*, 12−25.

(13) Bolotsky, A.; Butler, D.; Dong, C.; Gerace, K.; Glavin, N. R.; Muratore, C.; Robinson, J. A.; Ebrahimi, A. Two-Dimensional Materials in Biosensing and Healthcare: From In Vitro Diagnostics to Optogenetics and Beyond. *ACS Nano* **2019**, *13* (9), 9781−9810.

(14) Dai, W.; Zhang, J.; Wang, Y.; Jiao, C.; Song, Z.; Ma, Y.; Ding, Y.; Zhang, Z.; He, X. Radiolabeling of Nanomaterials: Advantages and Challenges. *Front Toxicol* **2021**, *3*, 753316.

(15) Dong, S.; Xia, T.; Yang, Y.; Lin, S.; Mao, L. Bioaccumulation of (14)C-Labeled Graphene in an Aquatic Food Chain through Direct Uptake or Trophic Transfer. *Environ. Sci. Technol.* **2018**, *52* (2), 541−549.

(16) Huang, C.; Xia, T.; Niu, J.; Yang, Y.; Lin, S.; Wang, X.; Yang, G.; Mao, L.; Xing, B. Transformation of (14) C-Labeled Graphene to (14) CO_2 in the Shoots of a Rice Plant. *Angew. Chem., Int. Ed. Engl.* **2018**, *57* (31), 9759−9763.

(17) Wyss, K. M.; Wang, Z.; Alemany, L. B.; Kittrell, C.; Tour, J. M. Bulk Production of Any Ratio (12)C:(13)C Turbostratic Flash Graphene and Its Unusual Spectroscopic Characteristics. *ACS Nano* **2021**, *15* (6), 10542−10552.

(18) *Toxicology of Nanomaterials*; Zhao, Y., Zhang, Z., Feng, W., Eds.; Wiley & Sons, USA, 2016; pp 1−432.

(19) Chaumeil, M. M.; Ozawa, T.; Park, I.; Scott, K.; James, C. D.; Nelson, S. J.; Ronen, S. M. Hyperpolarized ^{13}C MR spectroscopic imaging can be used to monitor Everolimus treatment in vivo in an orthotopic rodent model of glioblastoma. *NeuroImage* **2012**, *59* (1), 193−201.

(20) Kurhanewicz, J.; Bok, R.; Nelson, S. J.; Vigneron, D. B. Current and Potential Applications of Clinical ^{13}C MR Spectroscopy. *J. Nucl. Med.* **2008**, *49* (3), 341−344.

(21) Gallagher, F. A.; Woitek, R.; McLean, M. A.; Gill, A. B.; Manzano Garcia, R.; Provenzano, E.; Riemer, F.; Kaggie, J.; Chhabra, A.; Ursprung, S.; Grist, J. T.; Daniels, C. J.; Zaccagna, F.; Laurent, M. C.; Locke, M.; Hilborne, S.; Frary, A.; Torheim, T.; Boursnell, C.; Schiller, A.; al, e.; et al. Imaging breast cancer using hyperpolarized carbon-13 MRI. *Proc. Natl. Acad. Sci. U. S. A.* **2020**, *117* (4), 2092−2098.

(22) Yin, Y.; Tan, Z.; Hu, L.; Yu, S.; Liu, J.; Jiang, G. Isotope Tracers To Study the Environmental Fate and Bioaccumulation of Metal-Containing Engineered Nanoparticles: Techniques and Applications. *Chem. Rev.* **2017**, *117* (5), 4462−4487.

(23) Yu, J.; Lian, Y.; Xu, W.; Wang, C.; Chang, X.; Tang, T. B.; Gu, M. Proton conductance and dielectric relaxation in hydrated graphite oxide, studied with impedance spectroscopy. *Appl. Phys. Lett.* **2018**, *112* (17), 171603.

(24) Wang, Z.; Chang, X.; Lu, Z.; Gu, M.; Zhao, Y.; Gao, X. A precision structural model for fullerenols. *Chem. Sci.* **2014**, *5* (8), 2940−2948.

(25) Wang, C.; Ruan, L.; Chang, X.-L.; Zhang, X.; Yang, S.-T.; Guo, X.; Yuan, H.; Guo, C.; Shi, W.; Sun, B.; Zhao, Y. The isotopic effects of ^{13}C-labeled large carbon cage (C70) fullerenes and their formation process. *RSC Adv.* **2015**, *5* (94), 76949−76956.

(26) Valeš, V.; Verhagen, T.; Vejpravová, J.; Kalbáč, M. Raman spectroscopy and AFM study of ^{12}C graphene/fullerenes C70/^{13}C graphene heterostructure. *physica status solidi (b)* **2015**, *252* (11), 2418−2422.

(27) del Corro, E.; Kalbac, M.; Fantini, C.; Frank, O.; Pimenta, M. A. Isotopic$^{13}C/^{12}C$ effect on the resonant Raman spectrum of twisted bilayer graphene. *Phys. Rev. B* **2013**, *88* (15), 155436.

(28) Hu, B.; Ago, H.; Ito, Y.; Kawahara, K.; Tsuji, M.; Magome, E.; Sumitani, K.; Mizuta, N.; Ikeda, K.-i.; Mizuno, S. Epitaxial growth of large-area single-layer graphene over Cu(111)/sapphire by atmospheric pressure CVD. *Carbon* **2012**, *50* (1), 57−65.

https://doi.org/10.1021/acsnano.2c09799
ACS Nano 2023, 17, 606−620

(29) Carvalho, B. R.; Hao, Y.; Righi, A.; Rodriguez-Nieva, J. F.; Colombo, L.; Ruoff, R. S.; Pimenta, M. A.; Fantini, C. Probing carbon isotope effects on the Raman spectra of graphene with different C13 concentrations. *Phys. Rev. B* **2015**, *92* (12), 125406.
(30) Susi, T.; Hofer, C.; Argentero, G.; Leuthner, G. T.; Pennycook, T. J.; Mangler, C.; Meyer, J. C.; Kotakoski, J. Isotope analysis in the transmission electron microscope. *Nat. Commun.* **2016**, *7*, 13040.
(31) Whiteway, E.; Lee, M.; Hilke, M. Graphene Isotope Superlattices with Strongly Diminished Thermal Conductivity for Thermoelectric Applications. *ACS Applied Nano Materials* **2020**, *3* (9), 9167−9173.
(32) Ek-Weis, J.; Costa, S.; Frank, O.; Kalbac, M. Heating Isotopically Labeled Bernal Stacked Graphene: A Raman Spectroscopy Study. *J. Phys. Chem. Lett.* **2014**, *5* (3), 549−54.
(33) Wang, S.; Suzuki, S.; Hibino, H. Raman spectroscopic investigation of polycrystalline structures of CVD-grown graphene by isotope labeling. *Nanoscale* **2014**, *6* (22), 13838−13844.
(34) Frank, O.; Kavan, L.; Kalbac, M. Carbon isotope labelling in graphene research. *Nanoscale* **2014**, *6* (12), 6363−70.
(35) Chen, L.; Wang, C.; Li, H.; Qu, X.; Yang, S. T.; Chang, X. L. Bioaccumulation and Toxicity of (13)C-Skeleton Labeled Graphene Oxide in Wheat. *Environ. Sci. Technol.* **2017**, *51* (17), 10146−10153.
(36) González, V. J.; Rodríguez, A. M.; León, V.; Frontiñán-Rubio, J.; Fierro, J. L. G.; Durán-Prado, M.; Muñoz-García, A. B.; Pavone, M.; Vázquez, E. Sweet graphene: exfoliation of graphite and preparation of glucose-graphene cocrystals through mechanochemical treatments. *Green Chem.* **2018**, *20* (15), 3581−3592.
(37) González, V. J.; Rodríguez, A. M.; Payo, I.; Vázquez, E. Mechanochemical preparation of piezoelectric nanomaterials: BN, MoS2 and WS2 2D materials and their glycine-cocrystals. *Nanoscale Horizons* **2020**, *5* (2), 331−335.
(38) Beloin-Saint-Pierre, D.; Hischier, R. Towards a more environmentally sustainable production of graphene-based materials. *International Journal of Life Cycle Assessment* **2021**, *26* (2), 327−343.
(39) Gonzalez-Dominguez, J. M.; Leon, V.; Lucio, M. I.; Prato, M.; Vazquez, E. Production of ready-to-use few-layer graphene in aqueous suspensions. *Nat. Protoc* **2018**, *13* (3), 495−506.
(40) Leon, V.; Gonzalez-Dominguez, J. M.; Fierro, J. L.; Prato, M.; Vazquez, E. Production and stability of mechanochemically exfoliated graphene in water and culture media. *Nanoscale* **2016**, *8* (30), 14548−55.
(41) Del Rio-Castillo, A. E.; Merino, C.; Díez-Barra, E.; Vázquez, E. Selective suspension of single layer graphene mechanochemically exfoliated from carbon nanofibres. *Nano Research* **2014**, *7* (7), 963−972.
(42) Weisenberger, M.; Martin-Gullon, I.; Vera-Agullo, J.; Varela-Rizo, H.; Merino, C.; Andrews, R.; Qian, D.; Rantell, T. The effect of graphitization temperature on the structure of helical-ribbon carbon nanofibers. *Carbon* **2009**, *47* (9), 2211−2218.
(43) Martin-Gullon, I.; Vera, J.; Conesa, J. A.; González, J. L.; Merino, C. Differences between carbon nanofibers produced using Fe and Ni catalysts in a floating catalyst reactor. *Carbon* **2006**, *44* (8), 1572−1580.
(44) Reynier, Y.; Yazami, R.; Fultz, B.; Barsukov, I. Evolution of lithiation thermodynamics with the graphitization of carbons. *J. Power Sources* **2007**, *165* (2), 552−558.
(45) Tristan-Lopez, F.; Morelos-Gomez, A.; Vega-Diaz, S. M.; Garcia-Betancourt, M. L.; Perea-Lopez, N.; Elias, A. L.; Muramatsu, H.; Cruz-Silva, R.; Tsuruoka, S.; Kim, Y. A.; Hayahsi, T.; Kaneko, K.; Endo, M.; Terrones, M. Large area films of alternating graphene-carbon nanotube layers processed in water. *ACS Nano* **2013**, *7* (12), 10788−98.
(46) Yang, D. Q.; Sacher, E. Carbon 1s X-ray photoemission line shape analysis of highly oriented pyrolytic graphite: the influence of structural damage on peak asymmetry. *Langmuir* **2006**, *22* (3), 860−2.
(47) Bagri, A.; Mattevi, C.; Acik, M.; Chabal, Y. J.; Chhowalla, M.; Shenoy, V. B. Structural evolution during the reduction of chemically derived graphene oxide. *Nat. Chem.* **2010**, *2* (7), 581−7.
(48) Hontoria-Lucas, C.; López-Peinado, A. J.; López-González, J. d. D.; Rojas-Cervantes, M. L.; Martín-Aranda, R. M. Study of oxygen-containing groups in a series of graphite oxides: Physical and chemical characterization. *Carbon* **1995**, *33* (11), 1585−1592.
(49) Rozada, R.; Paredes, J. I.; Villar-Rodil, S.; Martínez-Alonso, A.; Tascón, J. M. D. Towards full repair of defects in reduced graphene oxide films by two-step graphitization. *Nano Research* **2013**, *6* (3), 216−233.
(50) Zhang, C.; Li, Q.; Tian, B.; Huang, Z.; Lin, W.; Li, H.; He, D.; Zhou, Y.; Cai, W. Isotope effect of the phonons mean free path in graphene by micro-Raman measurement. *Science China Physics, Mechanics & Astronomy* **2014**, *57* (10), 1817−1821.
(51) Anno, Y.; Takei, K.; Akita, S.; Arie, T. Artificially controlled synthesis of graphene intramolecular heterojunctions for phonon engineering. *physica status solidi (RRL) - Rapid Research Letters* **2014**, *8* (8), 692−697.
(52) Kalbáč, M.; Kavan, L.; Zukalová, M.; Dunsch, L. In Situ Raman Spectroelectrochemical Study of ^{13}C-Labeled Fullerene Peapods and Carbon Nanotubes. *Small* **2007**, *3* (10), 1746−1752.
(53) Ren, J.; Licht, S. Tracking airborne CO_2 mitigation and low cost transformation into valuable carbon nanotubes. *Sci. Rep.* **2016**, *6*, 27760.
(54) Fedoseeva, Y. V.; Okotrub, A. V.; Koroteev, V. O.; Borzdov, Y. M.; Palyanov, Y. N.; Shubin, Y. V.; Maksimovskiy, E. A.; Makarova, A. A.; Münchgesang, W.; Bulusheva, L. G.; Vyalikh, A. Graphitization of ^{13}C enriched fine-grained graphitic material under high-pressure annealing. *Carbon* **2019**, *141*, 323−330.
(55) Ferrari, A. C. Raman spectroscopy of graphene and graphite: Disorder, electron-phonon coupling, doping and nonadiabatic effects. *Solid State Commun.* **2007**, *143* (1−2), 47−57.
(56) Ferrari, A. C.; Basko, D. M. Raman spectroscopy as a versatile tool for studying the properties of graphene. *Nat. Nanotechnol.* **2013**, *8*, 235.
(57) Leon, V.; Quintana, M.; Herrero, M. A.; Fierro, J. L.; de la Hoz, A.; Prato, M.; Vazquez, E. Few-layer graphenes from ball-milling of graphite with melamine. *Chem. Commun. (Camb)* **2011**, *47* (39), 10936−10938.
(58) León, V.; Rodriguez, A. M.; Prieto, P.; Prato, M.; Vázquez, E. Exfoliation of Graphite with Triazine Derivatives under Ball-Milling Conditions: Preparation of Few-Layer Graphene via Selective Noncovalent Interactions. *ACS Nano* **2014**, *8* (1), 563−571.
(59) López-Díaz, D.; López Holgado, M.; García-Fierro, J. L.; Velázquez, M. M. Evolution of the Raman Spectrum with the Chemical Composition of Graphene Oxide. *J. Phys. Chem. C* **2017**, *121* (37), 20489−20497.
(60) Paton, K. R.; Varrla, E.; Backes, C.; Smith, R. J.; Khan, U.; O'Neill, A.; Boland, C.; Lotya, M.; Istrate, O. M.; King, P.; Higgins, T.; Barwich, S.; May, P.; Puczkarski, P.; Ahmed, I.; Moebius, M.; Pettersson, H.; Long, E.; Coelho, J.; O'Brien, S. E.; al, e.; et al. Scalable production of large quantities of defect-free few-layer graphene by shear exfoliation in liquids. *Nat. Mater.* **2014**, *13* (6), 624−630.
(61) Hao, Y.; Wang, Y.; Wang, L.; Ni, Z.; Wang, Z.; Wang, R.; Koo, C. K.; Shen, Z.; Thong, J. T. Probing layer number and stacking order of few-layer graphene by Raman spectroscopy. *Small* **2010**, *6* (2), 195−200.
(62) Chen, S.; Wu, Q.; Mishra, C.; Kang, J.; Zhang, H.; Cho, K.; Cai, W.; Balandin, A. A.; Ruoff, R. S. Thermal conductivity of isotopically modified graphene. *Nat. Mater.* **2012**, *11* (3), 203−7.
(63) Rourke, J. P.; Pandey, P. A.; Moore, J. J.; Bates, M.; Kinloch, I. A.; Young, R. J.; Wilson, N. R. The real graphene oxide revealed: stripping the oxidative debris from the graphene-like sheets. *Angew. Chem., Int. Ed. Engl.* **2011**, *50* (14), 3173−7.
(64) Varela-Rizo, H.; Rodriguez-Pastor, I.; Merino, C.; Martin-Gullon, I. Highly crystalline graphene oxide nano-platelets produced from helical-ribbon carbon nanofibers. *Carbon* **2010**, *48* (12), 3640−3643.

https://doi.org/10.1021/acsnano.2c09799
ACS Nano 2023, 17, 606−620

(65) Sahoo, M.; Antony, R. P.; Mathews, T.; Dash, S.; Tyagi, A. K. Raman studies of chemically and thermally reduced graphene oxide. *AIP Conf. Proc.* **2013**, *1512*, 1262.
(66) Vacchi, I. A.; Spinato, C.; Raya, J.; Bianco, A.; Menard-Moyon, C. Chemical reactivity of graphene oxide towards amines elucidated by solid-state NMR. *Nanoscale* **2016**, *8* (28), 13714−13721.
(67) Lucherelli, M. A.; Raya, J.; Edelthalhammer, K. F.; Hauke, F.; Hirsch, A.; Abellan, G.; Bianco, A. A Straightforward Approach to Multifunctional Graphene. *Chemistry* **2019**, *25* (57), 13218−13223.
(68) Wang, Z. M.; Hoshinoo, K.; Shishibori, K.; Kanoh, H.; Ooi, K. Surfactant-Mediated Synthesis of a Novel Nanoporous Carbon-Silica Composite. *Chem. Mater.* **2003**, *15* (15), 2926−2935.
(69) Cai, W.; Piner, R. D.; Stadermann, F. J.; Park, S.; Shaibat, M. A.; Ishii, Y.; Yang, D.; Velamakanni, A.; An, S. J.; Stoller, M.; An, J.; Chen, D.; Ruoff, R. S. Synthesis and solid-state NMR structural characterization of ^{13}C-labeled graphite oxide. *Science* **2008**, *321* (5897), 1815−7.
(70) Lerf, A.; He, H.; Forster, M.; Klinowski, J. Structure of Graphite Oxide Revisited. *J. Phys. Chem. B* **1998**, *102* (23), 4477−4482.
(71) Chen, X.; Xu, Z.-H.; Li, X.; Shaibat, M. A.; Ishii, Y.; Ruoff, R. S. Structural and mechanical characterization of platelet graphite nanofibers. *Carbon* **2007**, *45* (2), 416−423.
(72) Huff, L. A.; Tavassol, H.; Esbenshade, J. L.; Xing, W.; Chiang, Y. M.; Gewirth, A. A. Identification of Li-Ion Battery SEI Compounds through (7)Li and (13)C Solid-State MAS NMR Spectroscopy and MALDI-TOF Mass Spectrometry. *ACS Appl. Mater. Interfaces* **2016**, *8* (1), 371−80.
(73) Fischer, A.; Manefield, M.; Bombach, P. Application of stable isotope tools for evaluating natural and stimulated biodegradation of organic pollutants in field studies. *Curr. Opin Biotechnol* **2016**, *41*, 99−107.
(74) Frontinan-Rubio, J.; Gomez, M. V.; Gonzalez, V. J.; Duran-Prado, M.; Vazquez, E. Sublethal exposure of small few-layer graphene promotes metabolic alterations in human skin cells. *Sci. Rep* **2020**, *10* (1), 18407.
(75) Mu, Q.; Su, G.; Li, L.; Gilbertson, B. O.; Yu, L. H.; Zhang, Q.; Sun, Y. P.; Yan, B. Size-dependent cell uptake of protein-coated graphene oxide nanosheets. *ACS Appl. Mater. Interfaces* **2012**, *4* (4), 2259−66.
(76) Lammel, T.; Boisseaux, P.; Fernandez-Cruz, M. L.; Navas, J. M. Internalization and cytotoxicity of graphene oxide and carboxyl graphene nanoplatelets in the human hepatocellular carcinoma cell line Hep G2. *Part Fibre Toxicol* **2013**, *10*, 27.
(77) Contreras-Torres, F. F.; Rodriguez-Galvan, A.; Guerrero-Beltran, C. E.; Martinez-Loran, E.; Vazquez-Garza, E.; Ornelas-Soto, N.; Garcia-Rivas, G. Differential cytotoxicity and internalization of graphene family nanomaterials in myocardial cells. *Mater. Sci. Eng. C Mater. Biol. Appl.* **2017**, *73*, 633−642.
(78) Katsumiti, A.; Tomovska, R.; Cajaraville, M. P. Intracellular localization and toxicity of graphene oxide and reduced graphene oxide nanoplatelets to mussel hemocytes in vitro. *Aquat Toxicol* **2017**, *188*, 138−147.
(79) Newman, L.; Jasim, D. A.; Prestat, E.; Lozano, N.; de Lazaro, I.; Nam, Y.; Assas, B. M.; Pennock, J.; Haigh, S. J.; Bussy, C.; Kostarelos, K. Splenic Capture and In Vivo Intracellular Biodegradation of Biological-Grade Graphene Oxide Sheets. *ACS Nano* **2020**, *14* (8), 10168−10186.
(80) Wang, C.; Zhang, H.; Ruan, L.; Chen, L.; Li, H.; Chang, X.-L.; Zhang, X.; Yang, S.-T. Bioaccumulation of ^{13}C-fullerenol nanomaterials in wheat. *Environmental Science: Nano* **2016**, *3* (4), 799−805.

Recommended by ACS

Electrochemical Fine-Tuning of the Chemoresponsiveness of Langmuir–Blodgett Graphene Oxide Films
Juan M. Devida, Diego Pallarola, *et al.*
JULY 21, 2023
ACS OMEGA
READ

Biological Evaluation of Graphene Quantum Dots and Nitrogen-Doped Graphene Quantum Dots as Neurotrophic Agents
Akshaya Raghavan, Sutapa Ghosh, *et al.*
MAY 11, 2023
ACS APPLIED BIO MATERIALS
READ

Applications of Graphene in Five Senses, Nervous System, and Artificial Muscles
Jinbo Pang, Gianaurelio Cuniberti, *et al.*
JANUARY 19, 2023
ACS SENSORS
READ

Impact of the Interlayer Distance between Graphene and MoS_2 on Raman Enhancement
Lei Chen, Maurizio Prato, *et al.*
JUNE 29, 2023
CHEMISTRY OF MATERIALS
READ

Get More Suggestions >

https://doi.org/10.1021/acsnano.2c09799
ACS Nano 2023, 17, 606−620